Available online at www.sciencedirect.com

ScienceDirect

Energy Procedia 114 (2017) 3432 – 3444

Energy Procedia

13th International Conference on Greenhouse Gas Control Technologies, GHGT-13, 14-18 November 2016, Lausanne, Switzerland

Seismic modelling: 4D capabilities for CO_2 injection

P. Lubrano-Lavadera[a], Å. Drottning[ab], I. Lecomte[ab], B.D.E. Dando[a]*, D. Kühn[a], V. Oye[a]

[a]*NORSAR, Gunnar Randers Vei, N-2007 Kjeller, Norway*
[b]*University of Bergen,Department of Earth Science, PO BOX 7803, 5020 Bergen, Norway*

Abstract

This paper focuses on modelling the seismic response to a theoretical CO_2 injection into the upper reservoir at the Longyearbyen CO_2 Lab site in Svalbard, Norway. The modelling aims to assess the monitoring potential of a carbon capture and storage site. We demonstrate the effect of reservoir porosity and CO_2 concentration on seismic reflection amplitudes using a prestack depth migration simulator. In addition, we look at five different CO_2 plumes of increasing volume and model the seismic response as a proxy to monitoring the evolution of a CO_2 plume. We show that even low porosity reservoirs (2%) will generate a significant seismic response from the injection of CO_2, and that low CO_2 concentrations will also be detected. However, further increases in the CO_2 concentration will not be as simple to monitor, with the CO_2 contact providing the best seismic imaging potential. Furthermore, we demonstrate how illumination angle and hence seismic acquisition design is critical to avoid imaging artefacts.

Peer-review under responsibility of the organizing committee of GHGT-13.

Keywords: Seismic modelling; CCS monitoring; prestack depth migration; CO_2 injection; 4D seismic

1. Introduction

The Longyearbyen CO_2 Lab project was initiated in 2007 by The University Centre in Svalbard (UNIS), with the aim of converting the coal-fired power station in Longyearbyen on Svalbard (Norway), into a site for carbon capture and storage (CCS); ultimately transforming Svalbard into a CO_2 neutral community. Eight slim-hole exploration wells were drilled, fully cored and logged. Seismic surveys were completed and a microseismic monitoring network

* Corresponding author. Tel.: +47-468-13190.
E-mail address: ben@norsar.no

Peer-review under responsibility of the organizing committee of GHGT-13.
doi:10.1016/j.egypro.2017.03.1474

was deployed. Injection and fracture monitoring tests were completed in 2010 and 2013 to help understand the storage potential and fracture conductivity in addition to any potential seismic risk. Numerous geomechanical and modelling studies have been completed within the project (e.g. [1,2,3,4,5]).

The target siliciclastic reservoir for the CCS is located at a depth of 672-972 m, Late Triassic to Middle Jurassic in age. The reservoir is characterized by low to moderate matrix porosity (5-18%) and low permeability (>2 mD) [6], and can be divided into two formations. The upper ~25 m thick Knorringfjellet formation exhibits higher matrix porosity and permeability making it a better target for CO_2 injection, compared with the underlying ~275 m De Geerdalen formation [2].

This paper focuses on modelling the seismic response to a theoretical CO_2 injection into the upper reservoir as a means to improve monitoring of CCS sites. The modelling aims to demonstrate both the effect of reservoir porosity and CO_2 concentration on the seismic reflection amplitudes. In addition, we look at five different CO_2 plumes of increasing volume and model the seismic response using a novel prestack depth migration (PSDM) simulator.

2. Seismic modelling methodology

Seismic modelling typically involves the computation of synthetic seismograms either by ray-tracing (e.g. [7,8]), or finite difference (e.g. [9]). The synthetic seismograms must then be processed to generate the migrated seismic responses. Here we use a novel ray-based approach using a 3D prestack-depth convolution [10,11,12], which does not require the computational effort of computing synthetic seismograms. The method provides an estimation of the point scatterer response of a prestack depth migration at a reference point, which accounts for 3D resolution and illumination effects. The 3D convolution operator is called a Point Spread Function (PSF), and is generated from illumination vectors (difference between the slowness vectors from a shot and to a receiver [9]) at the reference point for a given survey design (i.e. multiple shots and receivers). The illumination vectors are combined with a selected wavelet to generate the PSDM filter in the wavenumber domain (i.e. the spatial frequency of a wave). By applying an inverse fast Fourier transform to this filter the PSF is generated, showing the imaging response in the spatial domain. Such PSFs may vary for different reference points throughout a target region depending on the survey geometry and the velocity model (and hence wave propagation effects), and thus need computing throughout the target region (full-field approach). However, if the variation between PSFs is small enough, it is possible to use a single computation (local target approach) to be representative for the entire target region.

In order to generate the final PSDM image, the PSF(s) must be convolved with a reflectivity cube for the target region that represents the elastic 4D changes imposed by the different CO_2 injection scenarios. Within this target we define the rock properties in terms of effective Vp, Vs, density, bulk modulus, shear modulus, and porosity, which can be derived from the well logs at the CO_2 Lab (e.g. [13]). Further, we also define values for water saturation and CO_2 concentration, together with the bulk modulus and density values of the brine and CO_2. Whereas values for mineral properties, e.g. quartz bulk modulus, shear modulus and density, are generally taken from published sources such as [14], the fluid properties vary with the actual fluid composition, and the temperature and pressure in target area. In order to quantify the fluid properties, we use the equations outlined in [15] for the brine properties whereas the CO_2 properties were quantified using [16]. Together these values are used to compute the overall effect on the elastic properties using the Gassmann equations [14]. They are simple and widely used equations for 4D rock physics modelling, and are known to provide useful results for clastic reservoirs even though they are based on the assumptions that both the solid and fluid phase are homogeneous and the pore space is interconnected:

$$K = K_{dry} + \frac{\left(1 - K_{dry}/K_{solid}\right)^2}{\phi/K_{fluid} + (1-\phi)/K_{solid} - K_{dry}/K_{solid}^{\,2}}, \quad \mu = \mu_{dry}, \rho = \phi\rho_{fluid} + (1-\phi)\rho_{solid}$$

where K, K_{dry}, K_{solid}, K_{fluid}, are the effective bulk moduli of the saturated rock, the dry rock, the mineral material making up the rock, and the pore fluid. ϕ is the porosity, μ and μ_{dry} are the effective shear modulus and the shear modulus of the dry rock, respectively, and ρ, ρ_{fluid} and ρ_{solid} are the average density, the fluid density and the density of the mineral making up the rock. The dry bulk modulus was parameterized using well data from CO2 Lab. From the effective elastic properties, the corresponding P-wave and S-wave velocities, and thus the reflectivity can be calculated.

2.1. Analytical PSDM filter with a local target approach

In creating a PSDM filter, an alternative to specifying a particular survey and full velocity model is to create an analytical PSDM filter from a maximum illumination dip and average velocity at the reference point [12]. The seismic response from such a filter is therefore independent from survey design and is a proxy for limited-aperture effects (survey and migration), as encountered in actual seismic acquisition. This method thus provides a simplified approach to test fundamental parameters, without the added complication of using a full background velocity model or specific survey design.

We generate an analytical PSDM filter and its corresponding PSF by combining a 30-Hz zero-phase Ricker wavelet with a maximum illumination dip of 30° (Fig. 1). For our target region, with a depth between 672 m to 697 m, such an illumination dip corresponds to a survey with approximately 800 m aperture. The resulting PSF is used with a local target approach (i.e. a single PSD throughout the target region).

The analytical filter and local target approach is used to first test the influence of reservoir porosity, CO_2 concentration, and effectiveness of imaging CO_2 plumes with different volumes. For the porosity and CO_2 concentration cases, a hypothetical reservoir model is used as shown in Fig. 2, with the reservoir divided into five layers of equal thickness (420 m).

To test the effect of porosity we create PSDM seismic images for three different cases: 2%, 5% and 10% porosity values. For each of these cases, the PSDM images are computed first with all layers of the reservoir saturated with brine (a ‘pre-injection’ image), and then with the upper three layers (i.e. 1260 m) saturated with CO_2, with brine in the layers below (a ‘post-injection’ image). A final image for each porosity case is computed to show the difference between the pre-injection and post-injection images.

For understanding the effect of CO_2 concentration on the PSDM images, we follow a similar approach to the porosity testing. We first compute a ‘pre-injection’ PSDM image where the full reservoir is saturated with brine. We compare this result with the ‘post-injection’ images for CO_2 concentrations of 5%, 10%, 15%, 20%, 25% and 100% within the upper three layers – again with brine saturating the layers below. For a final case, we apply a gradient concentration distributed over the upper four layers (with brine below), with CO_2 concentrations of 100%, 75%, 50%, and 25% in the respective layers (from the top). In all of these cases, the porosity within the reservoir is kept constant at 5%.

To evaluate the impact of CO_2 plumes of differing volume, we create five plume-shaped CO_2 distributions as shown in Fig. 3. The increase in extent of each plume is analogous to the evolution of a CO2 plume over time from continuing CO_2 injection. Each plume spans the full depth of the reservoir (at its centre), with maximum lateral extents of 1350 m, 1960 m, 2770 m, 3800 m, and 4370 m. In order to properly illuminate the steep sides of the CO_2 plumes, the maximum dip used in the PSDM filter was increased from 30° (for the porosity and concentration testing) to 45°. This corresponds to an increase in seismic survey aperture to 1500 m from the original 800 m. For each of the plumes, the CO_2 concentration is set to 100%, and the reservoir porosity to 5%. To demonstrate the effect on illumination angle (and hence survey aperture), we also show the effect on the PSDM images for illumination angles of 10° and 30° (survey apertures of 250 m and 800 m respectively).

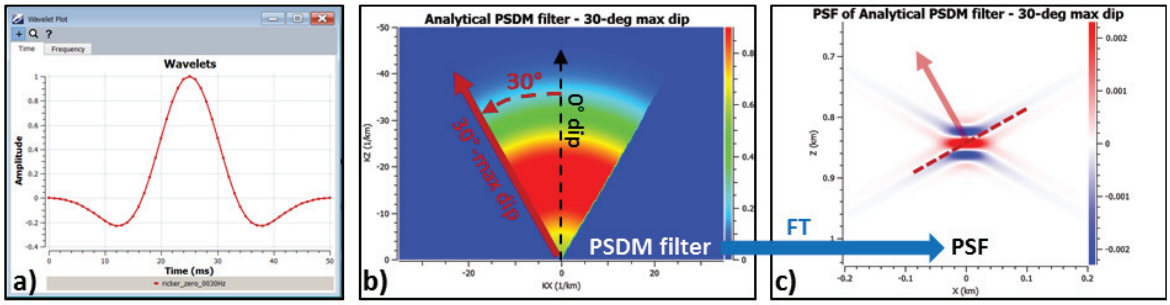

Fig. 1. (a) 30-Hz zero-phase Ricker wavelet (time domain); (b) vertical cross-section of a 3D analytical PSDM filter with a 30° maximum illumination dip: reflectors dipping up to 30° will be illuminated; (c) corresponding point spread function (PSF) after inverse Fourier transform of the PSDM filter: the cross-pattern of the PSF filter is generated by the 30° borders of the PSDM filter, where the branches of this pattern are at 90° from the PSDM filter borders.

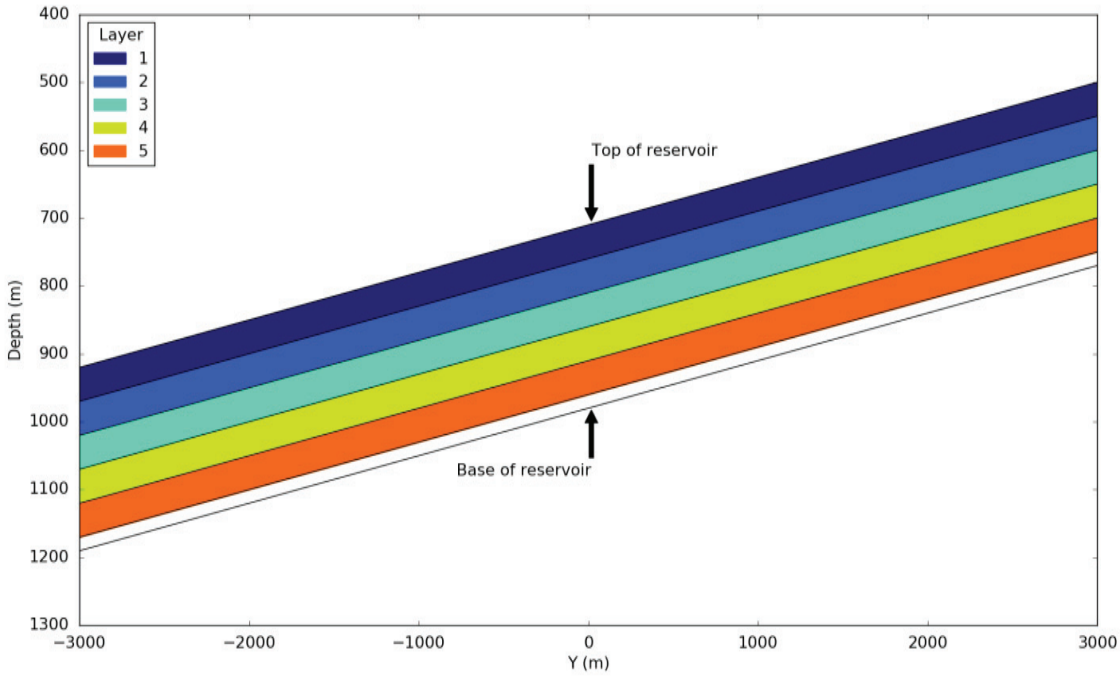

Fig. 2. Layered reservoir used in the seismic modelling to test the effect of porosity and CO_2 concentration.

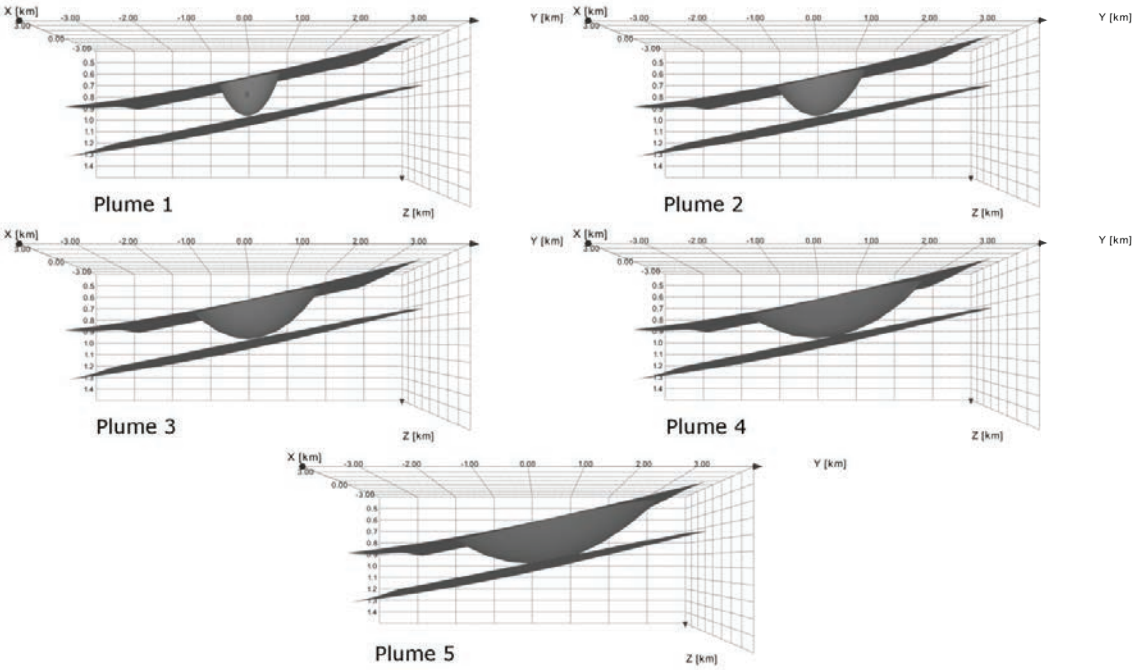

Fig. 3. Five CO_2 plumes of increasing volume. The top and bottom horizons show the extent of the reservoir.

3. Results

3.1. Influence of reservoir porosity

The PSDM images generated from the analytical PSDM filter workflow, and applied to the layered reservoir model in Fig. 2, are shown in Figs 4-6. Fig. 4 shows the results from using a porosity of 2%. On saturation of the upper three reservoir layers with CO_2, the CO_2/brine contact becomes visible within the seismic section. The difference plot between the CO_2 saturated section and the brine saturated reservoir shows a negative polarity at the top of the reservoir. This is due to a decrease in P-wave velocity with CO_2 saturation, which will therefore decrease the reflectivity. Conversely, at the base of layer 3, the introduction of the CO_2 creates an additional reflector with a positive impedance contrast, thus producing a positive polarity in the difference plot. As observed within Fig. 5 and Fig. 6 (porosity values of 5% and 10%, respectively), the greater the reservoir porosity, the higher the seismic amplitude this reflector will have.

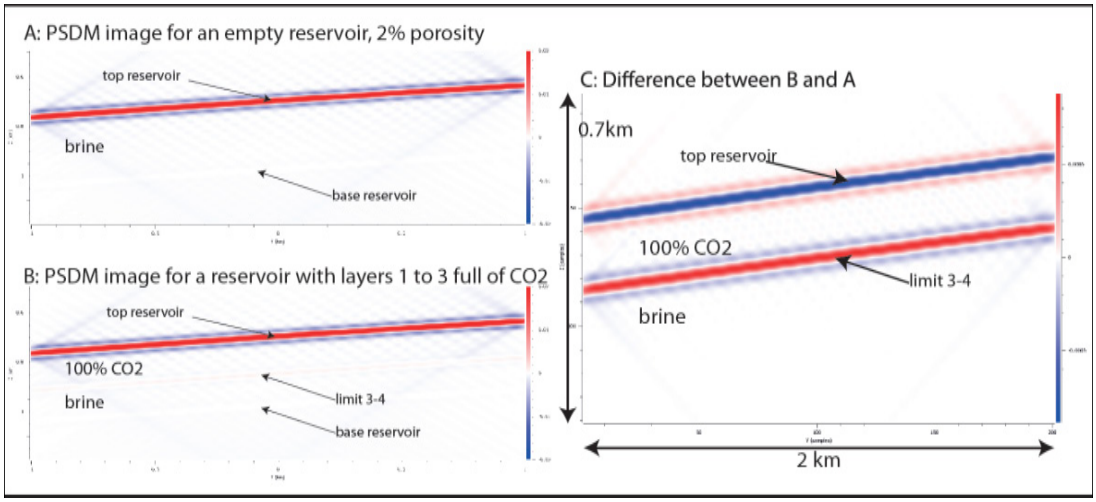

Fig. 4. PSDM seismic sections for a reservoir with porosity of 2%. (a) all reservoir layers are saturated with brine; (b) the upper three layers are saturated with CO2 with brine below; (c) difference between (b) and (a).

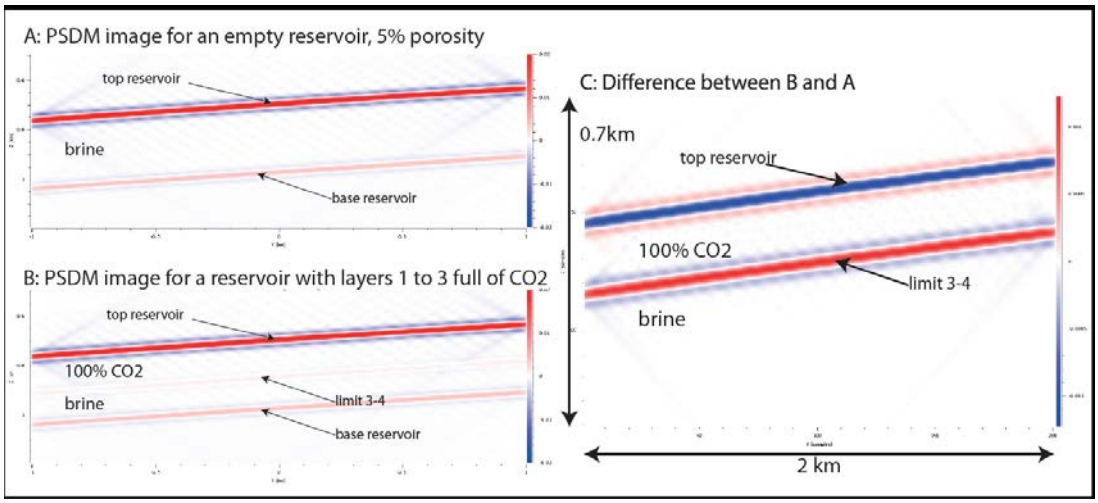

Fig. 5. PSDM seismic sections for a reservoir with porosity of 5%. (a) all reservoir layers are saturated with brine; (b) the upper three layers are saturated with CO_2 with brine below; (c) difference between (b) and (a).

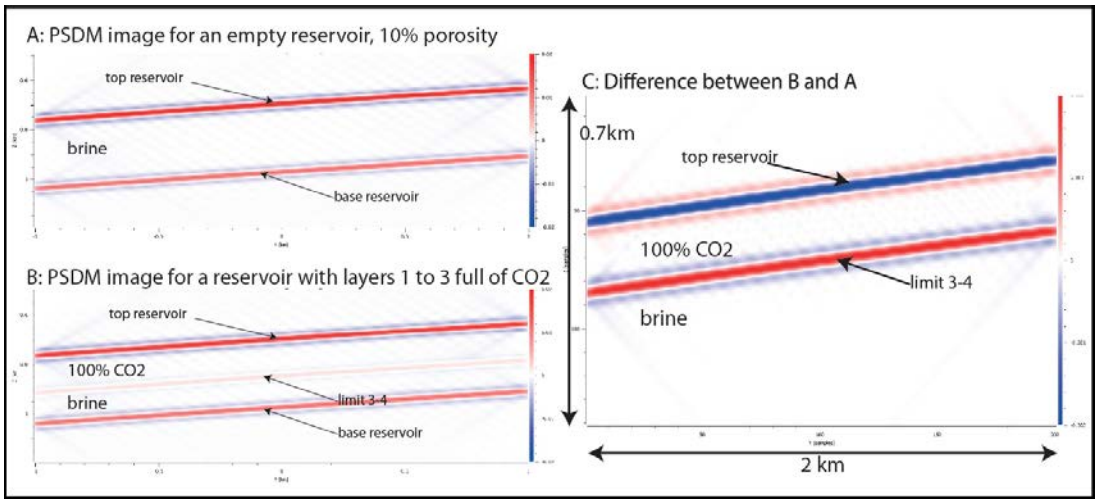

Fig. 6. PSDM seismic sections for a reservoir with porosity of 10%. (a) all reservoir layers are saturated with brine; (b) the upper three layers are saturated with CO_2 with brine below; (c) difference between (b) and (a).

3.2. Influence of CO_2 concentration

The effect of different CO_2 concentrations on the PSDM images is shown in Fig 7. For each of the cases where the CO_2 concentration is kept constant in the upper three layers (and above 0%), an additional reflector is observed at the layer 3 to layer 4 boundary. In the case of the gradient model, where CO_2 concentration varies from 100% at the top of the reservoir, down to 25% within layer 4, only the layer 4 to layer 5 boundary has a clear additional reflector, due to the high impedance contrast between the CO_2 and brine as compared with the gradual reduction in CO_2 within the top 4 layers.

Fig. 8 shows the difference plots between the different CO_2 concentrations, which illustrate how the biggest contrast for the reflector at the base of layer 3 occurs between the reservoir saturated with brine and then saturated with 10% CO_2 within the upper 3 layers. Further increases in the CO_2 concentration still show positive differences at this boundary, but the contrast is progressively reduced. This effect is due to the sensitivity of the bulk modulus to CO_2, so that going from no CO_2 to 10% has a large effect, but further increases have reduced effects on the bulk modulus, and thus reflectivity.

Fig. 8 also shows what was not apparent in Fig. 7 for the gradient CO_2 concentration case; that there are reflections between each of the individual layers. However, it reinforces the observation that increasing CO_2 concentration results in smaller increases in reflectivity – e.g. the reflection between the layer 1 and layer 2 boundary (100% and 75% CO_2 concentration, respectively), is much lower than between the layer 3 and layer 4 boundary (50% and 25% CO_2 concentration, respectively).

3.3. Imaging CO2 plumes

The impact of CO_2 plumes with varying volume on the PSDM seismic sections is shown in Fig. 9. For each of the plumes, where the lateral extent ranges from 1350 m for plume 1 to 4370 m for plume 5, the shape could be fully recovered using the analytical PSDM filter with a 45° maximum dip. This indicates that a survey with an aperture of ~1500 m is sufficient to effectively image CO_2 plumes with these extents. The effect of reducing the maximum illumination dip and thus seismic survey aperture, is illustrated in Fig. 10. It shows the results for both a 10° and 30° maximum dip in the PSDM filter (equivalent to approximate survey apertures of 250 m and 800 m respectively).

Only the first four plumes are shown. For the first three plumes, the flanks are relatively steep. This results in the plume being imaged incompletely for the 10° PSDM filter images. There are also artefacts below the plume due to the lack of range in the illumination angle. For the 30° PSDM filter images, the results are improved, with the plume flanks imaged at least for the larger plumes. However, plume 1, with the smallest extent and steepest flanks is still incomplete within the image. The results are significantly poorer than observed for the 45° PSDM filter images in Fig. 9.

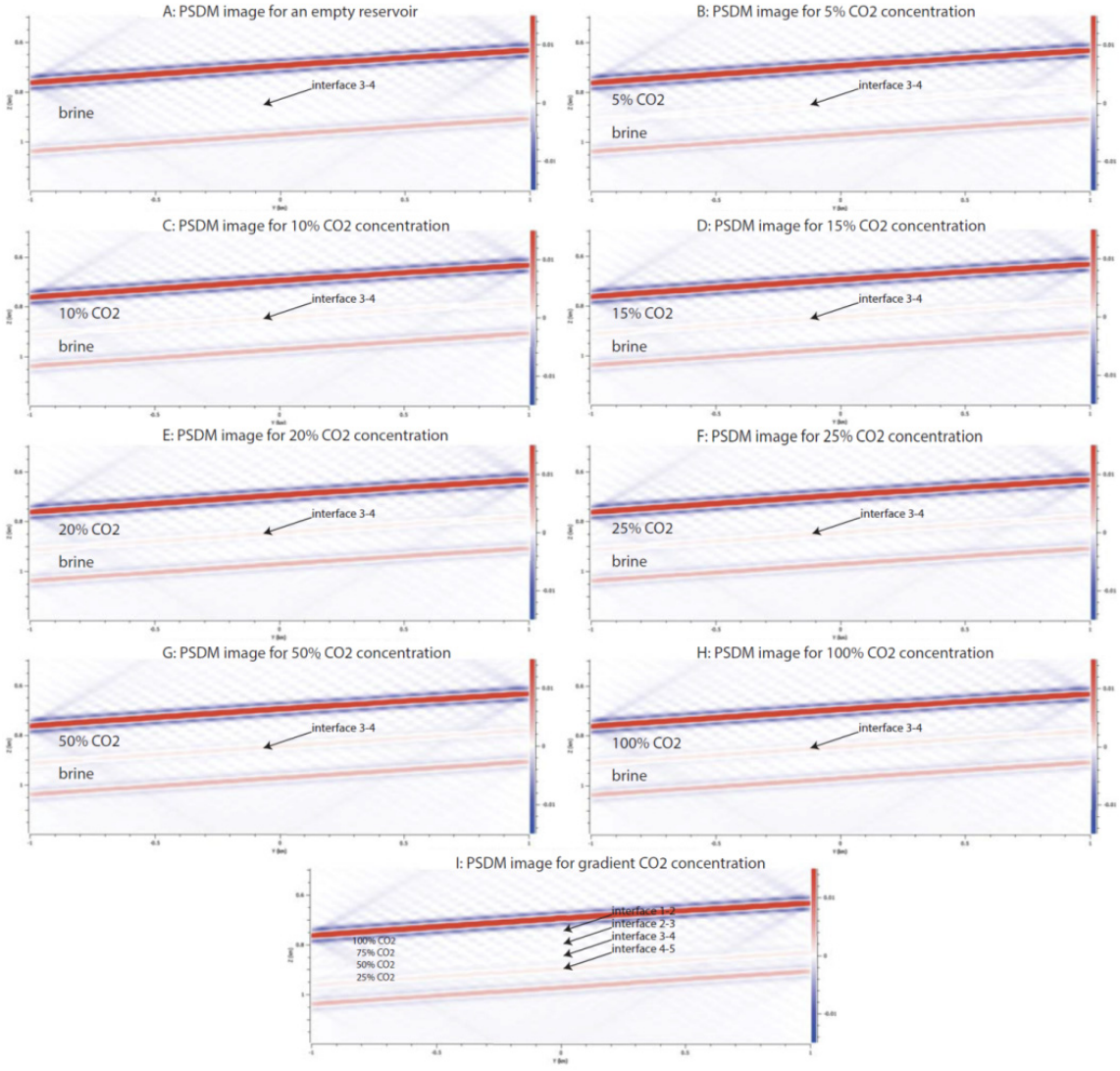

Fig. 7. PSDM seismic sections for a reservoir with different CO_2 concentrations (and a constant porosity of 5%). (a) no CO_2; (b) 5% CO_2 in the upper 3 layers; (c) 10% CO_2 in the upper 3 layers; (d) 15% CO_2 in the upper 3 layers; (e) 20% CO_2 in the upper 3 layers; (f) 25% CO_2 in the upper 3 layers; (g) 50% CO_2 in the upper 3 layers; (h) 100% CO_2 in the upper 3 layers; (i) a gradient from 100% CO_2 to 25% CO_2 in the upper 4 layers.

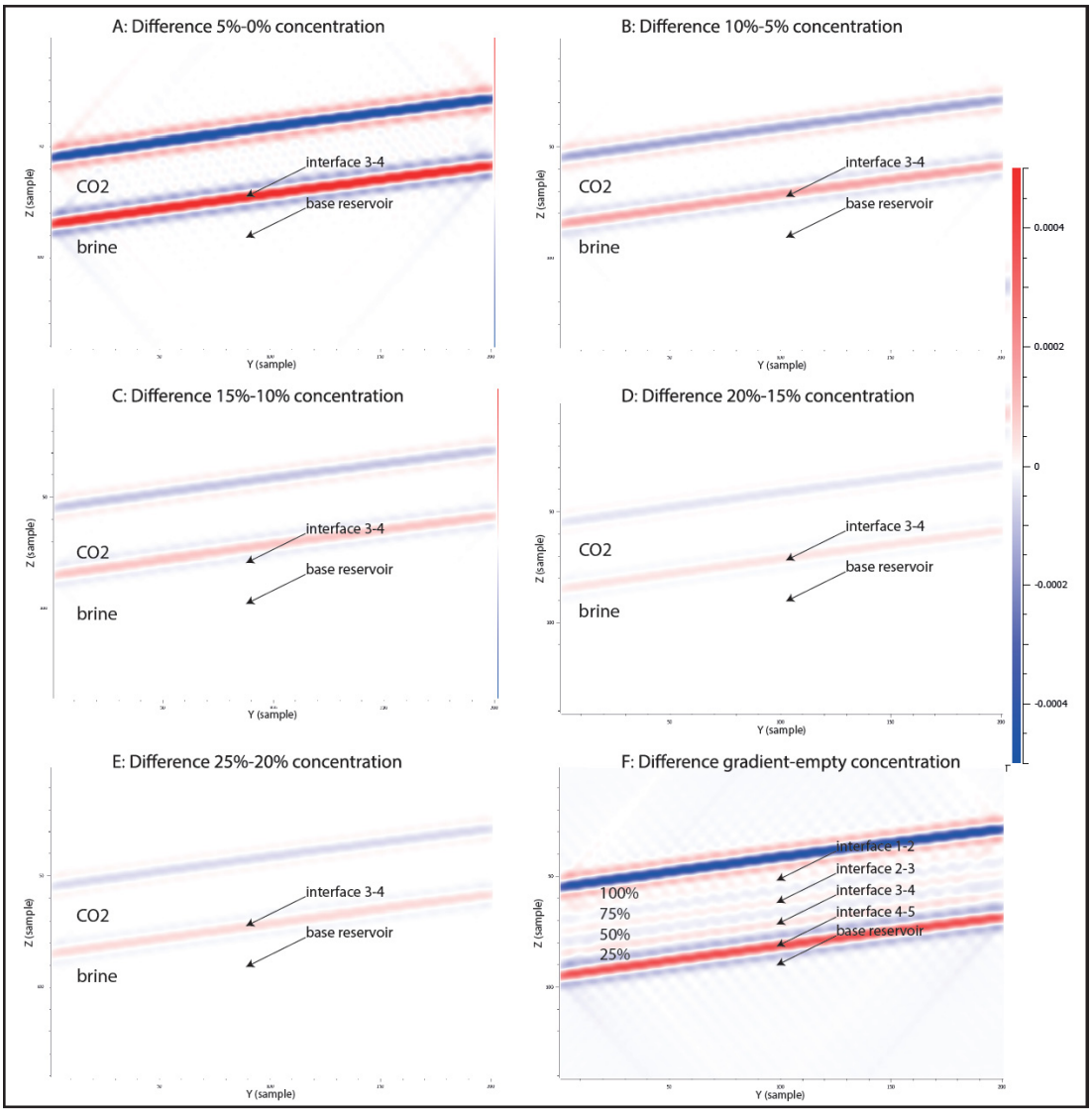

Fig. 8. Difference plots for PSDM seismic sections for a reservoir with different CO_2 concentrations (and a constant porosity of 5%). (a) difference between 0% and 5% CO_2 in the upper 3 layers; (b) difference between 5% and 10% CO_2 in the upper 3 layers; (c) difference between 10% and 15% CO_2 in the upper 3 layers; (d) difference between 15% and 20% CO_2 in the upper 3 layers; (e) difference between 20% and 25% CO_2 in the upper 3 layers; (f) difference between the reservoir fully saturated with brine and a gradient of CO_2 saturation from 100% CO_2 to 25% CO_2 in the upper 4 layers.

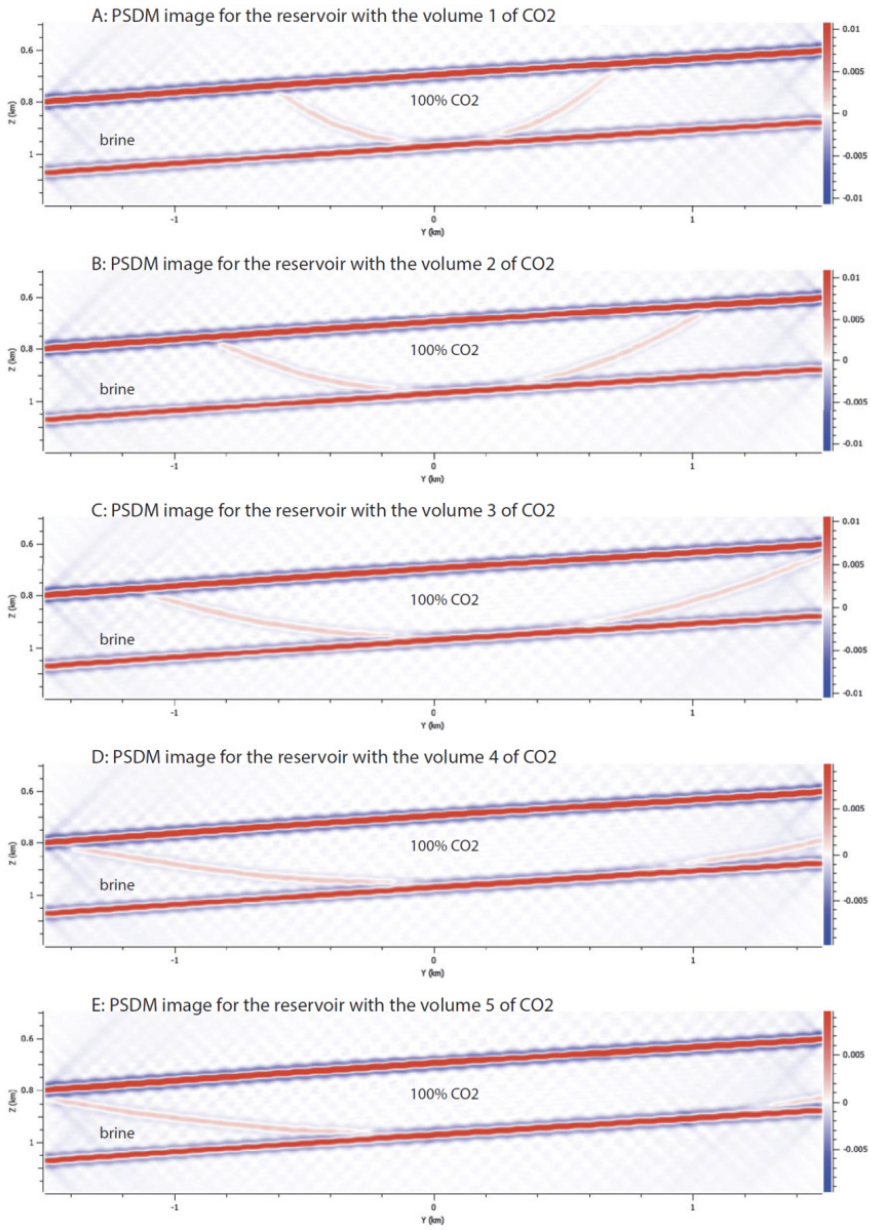

Fig. 9. PSDM seismic sections for 5 plumes with increasing CO_2 volume. The images are computed using an analytical PSDM filter with a maximum illumination dip of 45°. The CO_2 concentration within the plume is 100%, and the reservoir porosity is 5%.

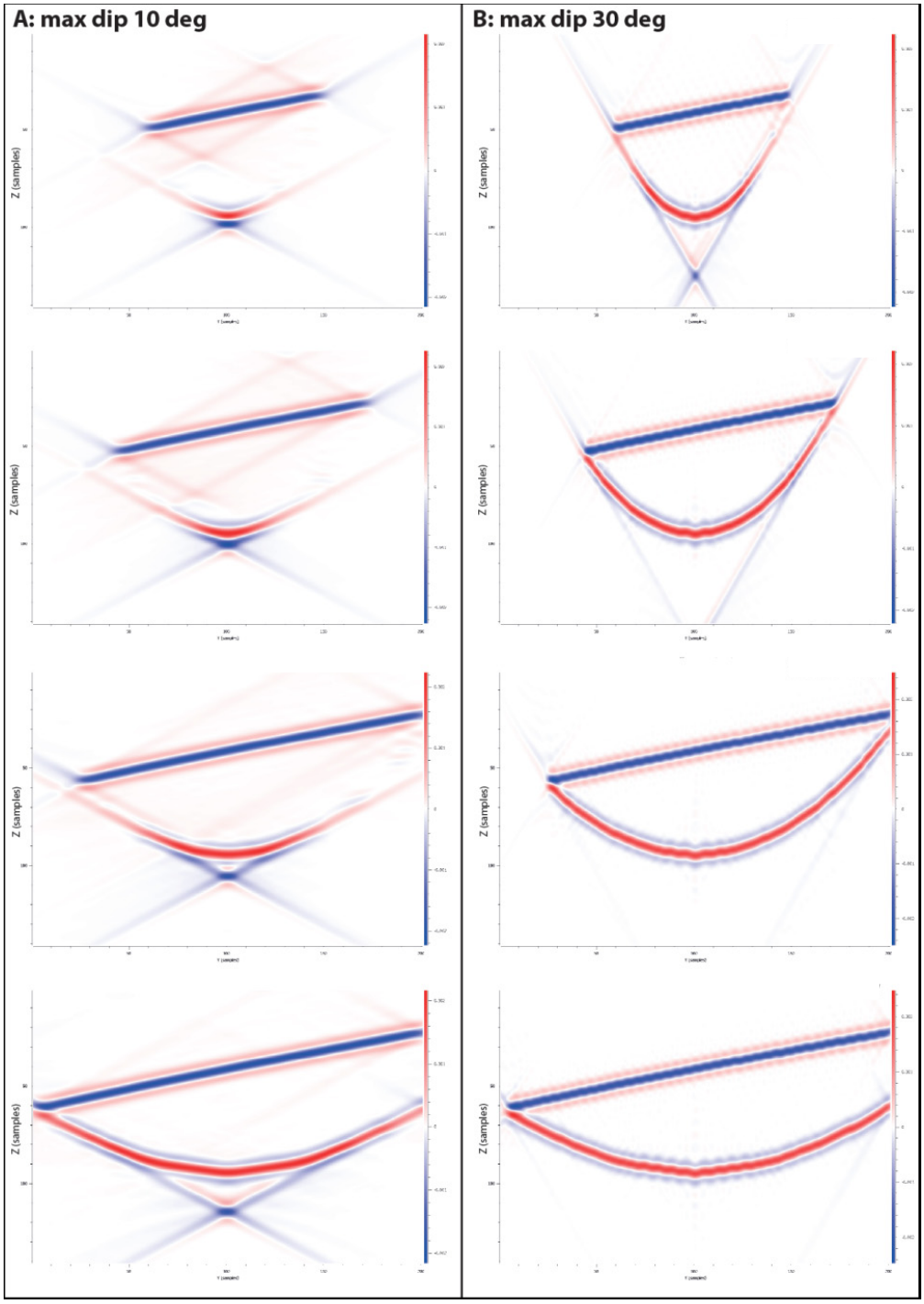

Fig. 10. Difference plots for PSDM seismic sections for the first 4 plumes with increasing CO_2 volume. The difference is between a reservoir fully saturated with brine, and a reservoir with the CO_2 plumes at 100% concentration. Left: difference plots for a PSDM filter with a maximum illumination dip of 10°. Right: difference plots for a PSDM filter with a maximum illumination dip of 30°.

4. Discussion and conclusions

Seismic monitoring of CCS sites is critical for understanding the storage capabilities of a reservoir, the spatial evolution of an injected CO_2 plume, and for the mitigation of potential seismic hazard. Key to such monitoring is an understanding of its limitations, and how the geology and seismic acquisition may affect the outcome. Seismic modelling provides an excellent means of testing such parameters without the need for expensive acquisitions.

In this study we have modelled the seismic response using an analytical PSDM filter to test the effect of reservoir porosity, CO_2 concentration, and CO_2 plumes of differing volume.

We have found that the introduction of CO_2 into a reservoir generates a significant seismic response even with a reservoir porosity of 2%. Increasing the reservoir porosity increases this response. In the context of the CO_2 Lab, where matrix porosity in the reservoir varies from 5-18%, this is clearly sufficient to observe a seismic response.

Testing the effect of increasing the CO_2 concentration within the reservoir on the seismic response has shown that there is a limited influence due to the sensitivity of the bulk modulus to CO_2. Low levels of CO_2 (e.g. 5% concentration) result in a significant seismic response when compared to an 'empty' (brine filled) reservoir. Further increases to the CO_2 concentration results in a reduction to the difference in the seismic response, due to a decay in the bulk modulus sensitivity. The implication for CCS monitoring is that seismic imaging will be limited in its ability to assess the amount of CO_2 within a reservoir. However, because the contact between CO_2 and brine is easily identifiable in the seismic response, the spatial extent of a CO_2 volume can be effectively monitored.

Applying the seismic modelling to CO_2 plumes of variable extent has shown that effective 3D illumination is required. In the case of using an analytical PSDM filter of 45°, which is equivalent to a seismic acquisition with a 1500 m aperture for our models, all five CO_2 plumes could be imaged without any significant artefacts. However, reducing the illumination angle to 30° (an acquisition with 800 m aperture) and then to 10° (an acquisition of 250 m aperture), for the CO_2 plumes with the steepest flanks it resulted in both artefacts in the images and incomplete imaging of the full extent of the plume volume. This highlights the importance of modelling to ensure that an effective seismic acquisition is designed in order for a CO_2 plume to be monitored throughout its evolution.

Acknowledgements

The work has been financed by Norwegian Research Council grants no. 189994 (SafeCO2 project) and 224880 (SafeCO2-II project). The projects have been sponsored additionally by our industry partners Lundin, Octio, READ and Statoil (SafeCO2) as well as Lundin, RWE DEA Norge and Statoil (SafeCO2-II). We would also like to thank Tina Kaschwich for helpful discussions in completing this work and for help in developing the models within the NORSAR-3D software package. Finally, we would like to thank UNIS and CO_2 Lab for access to data and valuable input.

References

[1] Sand G., Braathen A., Olaussen S. Longyearbyen CO_2 Lab – tales of research and eductation. Norwegian Journal of Geology; 2014; 94; pp. 77-82.

[2] Braathen A., Bælum K.., Christiansen H., Dahl T., Eikan O., Elvebakk H., Hansen F., Hanssen T.H., Jochmann M., Johansen T.A., Johnsen H., Larsen L., Lie T., Mertes J., Mørk A., Mørk M.B., Nemec W., Olaussen S., Oye V., Rød K., Titlestad G.O., Tveranger J., Vagle K.. The Longyearbyen CO_2 Lab of Svalbard, Norway – initial assessment of the geological conditions for CO_2 sequestration. Norwegian Journal of Geology 2012; 92; pp. 353-376.

[3] Bohloli B., Skurtveit E., Grande L., Titlestad G.O., Børresen M.H., Johnsen Ø., Braathan A. Evaluation of reservoir and cap-rock integrity for the Longyearbyen CO_2 storage pilot based on laboratory experiments and injection tests. Norwegian Jouranal of Geology; 2014; 94; pp. 171-187.

[4] Farokhpoor R., Torsater O., Baghbanbashi T., Mørk A., Lindeberg E.G.B. Experimental and numerical simulation of CO_2 injection into Upper-Triassic Sandstones in Svalbard, Norway. SPE International Conference on CO_2 Capture, Storage, and Utilization; 2010; SPE 139524; doi: 10.2118/139524-MS.

[5] Senger K., Tveranger J., Braathen A., Olaussen S., Ogata K., Larsen L. CO_2 storage resource estimates in unconventional reservoirs: insights from a pilot-sized storage site in Svalbard, Arctic Norway. Environmental Earth Sciences; 2015; 73; 8; pp. 3987-4009.

[6] Mørk M.B.E. Diagenesis and quartz cement distribution of low-permeability Upper Triassic–Middle Jurassic reservoir sandstones, Longyearbyen CO_2 lab well site in Svalbard, Norway. AAPG Bulletin; 2013; 97: 577–596.
[7] Cerveny V., Molotkov J.A., Psencik I. Ray method in seismology. Charles University Press, Prague; 1977.
[8] Cerveny V. Seismic ray theory. Cambridge University Press; 2001.
[9] Virieux J. P-SV wave propagation in heterogeneous media: velocity-stress finite-difference method. Geophysics; 1986; 51; 4; pp. 889-901.
[10] Lecomte I. Resolution and illumination analyses in PSDM: a ray-based approach. The Leading Edge; 2008; 27(5); 650-663; doi: 10.1190/1.2919584.
[11] Lecomte I., Lubrano Lavadera P., Anell I., Buckley S.J., Schmid D.W., Heeremans M. Ray-based seismic modeling of geologic models: understanding and analyzing seismic images efficiently. Interpretation; 2015; 3(4); SAC71-SAC89; doi: 10.1190/INT-2015-0061.1.
[12] Lecomte I., Lubrano Lavadera P., Botter C., Anell I., Buckley S.J., Eide C.H., Grippa A., Mascolo V., Kjoberg S. 2(3)D convolution modelling of complex geological targets - beyond 1D convolution. First Break; 2016; 34(5); pp. 99-107.
[13] Bælum K.., Johansen T.A., Johnsen H., Rød H., Ruud B.O., Braathen A. Subsurface structures of the Longyearbyen CO2 Lab study area in Central Spitsbergen (Arctic Norway), as mapped by reflection seismic data. Norwegian Journal of Geology; 2012; 92; pp. 377-389.
[14] Mavko G., Mukerji T., Dvorkin J. The Rock Physics Handbook: Tools for Seismic Analysis of Porous Media; Cambridge University Press; 2009.
[15] Batzle M., Wang Z. Seismic properties of pore fluids. Geophysics; 1992; 57; 11; p. 1396-1408.
[16] Span R., Wanger W. A new equation of state for Carbon Dioxide covering the fluid region from the triple point temperature to 1100K at pressures up to 800 MPa; The Journal of Physical Chemistry; 1996; 25; 1509-1596.